Int. J. Heat Mass Transfer. Vol. 28, No. 8, pp. 1441–1450, 1985
Printed in Great Britain

0017-9310/85 $3.00 + 0.00

Droplet evaporation by combined mechanisms in an ICF reactor

H. KISLEV* and A. NIR
Department of Chemical Engineering, Technion—Israel Institute of Technology, Haifa 32000, Israel

(*Received* 26 *September* 1983 *and in final form* 3 *January* 1985)

Abstract—The heat transfer from dense steam plasma to a moving spherical water droplet has been computed using a self-similar solution for an optically thick boundary layer. Simultaneous radiation, vapor dissociation, convection, conduction and blowing were considered. The droplet evaporation rate has been computed for several pressures and temperatures and compares well with known rates at low temperature and atmospheric pressure. The results were incorporated into a model describing the cooling process of a stagnant steam fireball predicted for an ICF reactor.

1. INTRODUCTION

DROPLET evaporation appears in many industrial processes such as combustion, spray cooling or spray drying. The calculation of the rate of evaporation in these sprays is usually analyzed by assuming that each droplet is independent of the presence of the others [1–3]. Ensembles of droplets are grouped by their size and range, while the evaporation rate within a group is determined using the heat transfer coefficient of a typical droplet having an average size in that group. Radiative heat transfer to droplets is rarely included in such computations. Yet, in situations involving environments such as in various postulated Inertial Confinement Fusion (ICF) reactors [4, 5] with very high ambient temperatures far exceeding those associated with fuel combustion, the radiative heat transfer can be significant or dominant. Kislev [4] and Kislev and Micklich [6] suggested a concept for a light ion beam ICF reactor in which pressurized boiling water is used as an internal blanket (see Fig. 1) and where frequent consecutive pellet explosions are carried out. Since high pressure steam is present in the vortex cavity, every pellet explosion produces a dense concentric fireball. Such a fireball contains dissociated water molecules and is considered to be highly corrosive and thus, should be rapidly cooled before it comes in contact with the inner parts of the reactor.

During a fireball cooling cycle, explosion-induced water splashes emerge from the cavity wall, enter the plasma and evaporate rapidly causing a specific enthalpy decrease [7]. Extrapolating the available data for steam plasma emissivity [8] indicates values between 0.1 and 1 at the relevant parameters region, i.e. 0.2 to 0.8 eV. This suggests that heat transfer calculations must consider radiation as well as convection and conduction. The evaporation of the fast moving water droplets takes place across a thermal boundary layer. The high ambient temperature causes an intense evaporation which is translated to a blowing effect at the droplet surface. Furthermore, a dissociation of water molecules occurs within the boundary layer and renders steep nonlinear variations of the properties of the water plasma which can no longer be described via power-law correlations [9]. Exact correlations of water properties across the boundary layer must be incorporated to evaporation calculations.

Since the surface tension of water is high even in elevated temperature it is assumed that the small droplets caused by the water splashes which enter the fireball are spherical. In this case the heat transfer problem can be reduced to a description of an axisymmetric boundary layer over a sphere. A model involving simultaneous conduction, convection, radiation and blowing for this case has not yet been presented. There are several self-similar solutions for a boundary layer over axisymmetric moving bodies with blowing but without radiation [10]. Dombrovski has developed some models for radiative transfer over isothermal plate where the boundary layer is optically thin and with surface blowing [11] or when the boundary layer is optically thick [12]. Azad and Modest [13] have developed a model for calculating heat transfer between radiation flowing gas and circular tube where the boundary layer is described by an empirical correlation rather than a self similar solution. The gas properties were assumed temperature independent. There are some works in which empirical correlation for convective heat transfer from an evaporating sphere were used and the radiation flux was computed separately and superimposed on the equations in an iterative manner. These methods assume an optically thin boundary layer and their relevance to our problem is limited [1, 3].

In this paper we present an evaluation of the equations of the boundary layer over a water droplet which is rapidly evaporating by simultaneous mechanisms. The high emissivity of steam plasma indicates that in the boundary layer it has a high extinction coefficient, e.g. approx. 2×10^4 m^{-1} at 8 MPa

* Present address: Nuclear Engineering Program, University of Illinois at Urbana—Champaign, IL 61801, U.S.A.

NOMENCLATURE

A	injection parameter
$a_{1,2,3}$	coefficients in equation (22)
Bo	Boltzman number, $H_\infty \rho_e V_e/\sigma T_e^4$
C_D	drag coefficient
C_p	heat capacity at constant pressure
D	droplet diameter
f	dimensionless stream function, $f' = 2V/V_e$
g	gravitational acceleration
H	total enthalpy
k	thermal conductivity
L	ratio of the density–viscosity product across the boundary layer, $\frac{\rho\mu}{\rho_e\mu_e}$
M	Mach number
N	dimensionless conduction radiation parameter, $\frac{\Sigma k}{4\sigma\Gamma_e^3}$
Nu	Nusselt number
P_0	static pressure
q	heat flux
r	radial coordinate
R	droplet radius
Re	Reynolds number
r_b	fireball radius
r_k	characteristic radius
s	droplets cumulative number
T	temperature
t	time
V	velocity
w, w_t	cumulative and total water mass entering the fireball
x, y	tangential and normal coordinate of the boundary layer.

Greek symbols

α	heat diffusivity coefficient
β	Falkner–Skan coefficient
δ_h, δ_T	velocity and thermal boundary-layer thickness, respectively
θ	angle from the droplet velocity vector
λ	heat of evaporation
η	similarity variable $0.5(\rho_e V_e/\mu_e x)^{1/2}\int_0^y \frac{\rho}{\rho_e}\,dy$
μ	viscosity
Σ	optical extinction coefficient
σ	Boltzman emissivity constant
ρ	density
τ, τ_x	optical radial and tangential coordinates.

Superscripts

$'$	differentiation with respect to η
$-$	dimensionless
$\hat{}$	variable expectancy value.

Subscripts

e, w	conditions at the edge of the boundary layer and on the surface respectively
f	average film property
i	initial
L	liquid
r, θ	radial and tangential components, respectively
rad	radiative
∞	free-stream value.

and 3000 K [14]. By extrapolating these data to the relevant region (0.2–0.8 eV) and using Dombrovski [11] criterion for the significance of the radiative heat transfer contribution it is deduced that the boundary layer can be considered optically thick. Although layer zones which are beyond ~0.6 eV experience a dramatic reduction in the local absorption coefficient the remainder of the layer is still optically thick so that the total resistance to heat transfer remains similar. Hence, the photon mean free path is smaller than the boundary-layer thickness, the radiation does not penetrate to the evaporating surface and its flux is independent of the surface geometry [12]. It follows that a self-similar solution to the boundary layer equations is applicable [12].

The use of classical boundary-layer equations to evaluate heat transfer from dense plasma to isothermal cold bodies was investigated by Eckert and Pfender [15] who found minor changes in the Nusselt number for ionized gases over a wide range of physical parameters.

In Section 2 we describe the basic equations. In Section 3 we outline a model for the use of the evaporation rate of a single droplet to analyze the cooling rate of a fireball. The numerical algorithm is described in Section 4 while results and discussion follow.

2. THE BASIC EQUATIONS

Following Dewey and Gross [9], the mass, momentum and energy balances are of the form

$$\frac{\partial}{\partial x}(\rho V_\theta r) + \frac{\partial}{\partial y}(\rho V_r r) = 0 \tag{1}$$

$$\rho V_\theta \frac{\partial V_\theta}{\partial x} + \rho V_r \frac{\partial V_\theta}{\partial y} = \frac{\partial P}{\partial x} + \frac{1}{r}\frac{\partial}{\partial y}\left(\mu r \frac{\partial V_\theta}{\partial y}\right); \quad \frac{\partial P}{\partial y} = 0 \tag{2}$$

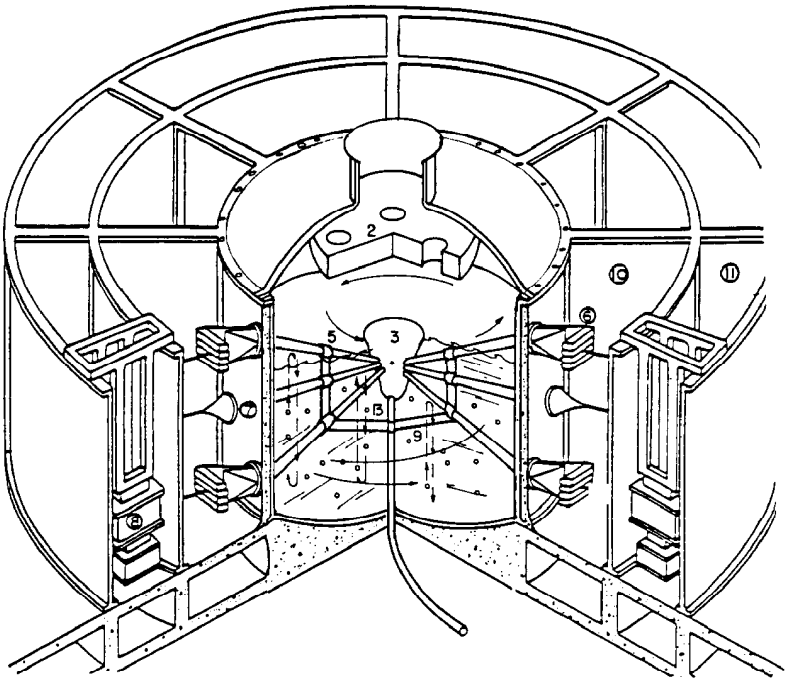

FIG. 1. A schematic diagram of the heavy water reactor concept.

$$\rho V_\theta \frac{\partial H}{\partial x} + \rho V_r \frac{\partial H}{\partial y} = \frac{1}{r}\frac{\partial}{\partial y}\left(r\frac{\mu}{Pr}\frac{\partial H}{\partial y}\right) + \frac{1}{r}\frac{\partial}{\partial y}\left[r\mu\left(1-\frac{1}{Pr}\right)\frac{\partial}{\partial y}\left(\frac{V_\theta^2}{2}\right)\right] - \left(\frac{\partial q_x}{\partial x} + \frac{\partial q_r}{\partial y}\right). \quad (3)$$

Here x and y are local coordinates along the spherical surface (Fig. 2). The equation for the enthalpy (3) is modified to incorporate radiation into the model. The following assumptions are made:

(a) The droplet maintains a spherical shape.
(b) Boundary-layer variables are self similar.
(c) The droplet is surrounded by an isothermal fireball gas.
(d) The liquid in the droplet is maintained in a uniform saturation temperature.
(e) Forces on the droplet in the fireball involve gravity and aerodynamic drag only. We neglect electromagnetic fields and possible radiation pressures.
(f) The extinction coefficient corresponds to the Rosseland mean free path and is held constant throughout the boundary layer.

Applying these assumptions, equations (1)–(3) are subject to the boundary conditions

$$\begin{aligned} &y = 0 \quad T = T_0 \quad V_\theta = 0 \\ &y = \infty \quad T = T_\infty \quad \frac{\partial T}{\partial y} = 0 \\ &V_\theta = V_\infty \quad V_r = 0. \end{aligned} \quad (4)$$

The equations and conditions (1)–(4) governing the steady laminar compressible boundary layer around a sphere with blowing can be rendered nondimensional by introducing the following definitions [10]

$$\eta = \frac{1}{2}\left(\frac{\rho_e V_e}{\mu_e x}\right)^{1/2}\int_0^y \frac{\rho}{\rho_e}\,dy;$$

$$L = \frac{\rho\mu}{\rho_\infty \mu_\infty}; \quad \bar{q}_r = \frac{q_r}{4\sigma T_\infty^4}; \quad \bar{T} = T/T_\infty$$

$$N = \frac{\Sigma k}{4\sigma T_\infty^3}; \quad \tau = \Sigma\int_0^y \frac{\rho}{\rho_e}\,dy;$$

$$\tau_x = \frac{\Sigma\sigma T_e^4}{V_\infty \rho_\infty H_\infty}\int_0^x \frac{\rho}{\rho_e}\,dx. \quad (5)$$

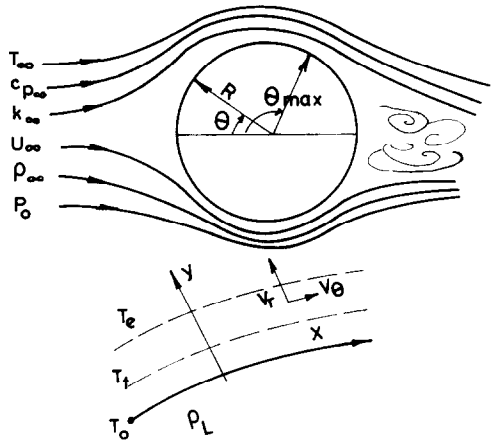

FIG. 2. A droplet moving and evaporating in an isothermal field.

Hence, the momentum balance becomes the familiar Falkner–Skan equation

$$(Lf'')'+ff''=\beta\left(f'^2-\frac{4\rho_e}{\rho}\right) \tag{6}$$

with

$$\beta=2\theta\frac{V_e'}{V_e}\frac{d\eta}{d\theta},$$

while the energy equation obtains the form

$$\left(\frac{kH'}{C_p}\right)'+fH'+4\left[\left(\mu-\frac{k}{C_p}\right)M^2f'^2\right]'H_e = 4T_\infty k\tau_x\frac{\partial\bar{q}_r}{\partial\tau}Pr. \tag{7}$$

In equation (5) N describes a dimensionless conduction–radiation parameter while τ and τ_x denote optical coordinates across and along the boundary layer, respectively.

The above equations can be further simplified using the additional assumptions:

(f) The steady laminar boundary layer is thin compared to the droplet radius.
(g) The Mach number of the droplet is much smaller than unity. This is used to neglect the third term in the LHS of equation (7).
(h) The resistance to heat transfer is concentrated in the boundary layer.
(i) Density–viscosity product across the boundary layer is unchanged $L=1.0$.
(j) No radiation reaches into the droplet.

For an optically thick boundary layer we can use the radiation–'conduction' approximation [12]

$$\bar{q}_r=-\frac{4}{3}\frac{\partial\bar{T}^4}{\partial\tau}. \tag{8}$$

The enthalpy is expressed in terms of the temperature by

$$H'=\bar{T}'T_\infty C_p. \tag{9}$$

Substituting equations (8) and (9) in equations (6) and (7) yields

$$f'''+ff''=\beta\left[(f')^2-4\frac{\rho_e}{\rho}\right] \tag{10}$$

$$\frac{(k\bar{T}')'}{k}+Prf\bar{T}'=-\frac{4}{3N}(\bar{T}'\bar{T}^3)' \tag{11}$$

subject to the following boundary conditions

$$f'(0)=0,\quad f'(\infty)=2,\quad \bar{T}(0)=T_0/T_\infty,\ \bar{T}(\infty)=1 \tag{12}$$

where $\beta=0.5$ for a sphere [14].

The values of f and $\bar{T}'$ on the droplet surface $f(0)$, $\bar{T}'(0)$ which are associated with the local blowing velocity and evaporation rate, respectively, are connected by

$$f(0)=-\frac{T_\infty k_0 r_k\bar{T}'(0)}{2\lambda\mu_0} \tag{13}$$

Analysis of the expression $(\bar{T}'k)'/k$ leads to the conclusion that the contribution of the component involving the conductivity gradient is relatively negligible and thus the first term in LHS of equation (11) becomes $\bar{T}'''$ [12]. Equations (10) and (11) with the boundary conditions (12) constitute the problem for solution.

The numerical scheme

A numerical integration of the boundary-layer equations [5] was obtained by solving them as an initial value problem assuming appropriate estimates for the conditions $\bar{T}'(0)$ and $f''(0)$. The evaluated conditions at the edge of the boundary layer, $\bar{T}(\infty)$ and $f'(\infty)$ were incorporated into a target function

$$F[\bar{T}'(0),f''(0)]=\exp|f(\infty)-2|+\exp(2|\bar{T}(\infty)-1|) \tag{14}$$

which was subsequently minimized. Initial guesses of $\bar{T}'(0)$ and $f''(0)$ for this shooting method were calculated by applying the correlation for heat transfer from a non-evaporating droplet used by [3] and the data of [1] associated with the solution of the hydrodynamic boundary layer over a flat plate ($\beta=0$). The optimization algorithm searches the initial condition domain using the Flatcher–Powell method. In most cases integration up to $\eta=10$ proved sufficient for convergence. Dombrovski [12], solving the boundary-layer equations using an iterated double sweep procedure with Pohlhausen profile as a zeroth approximation, extended to $\eta=20$ in most cases of his calculation.

Droplet heat and mass transfer

We describe here some of the results related to the structure of the boundary layer formed around the

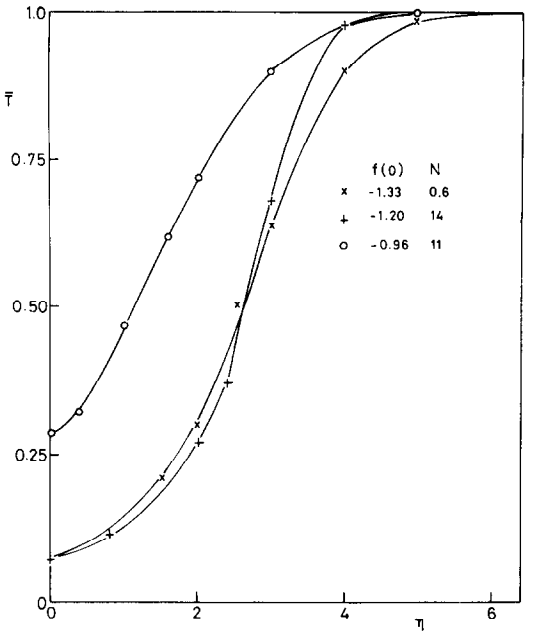

FIG. 3. Typical temperature profiles in the boundary layer.

droplet during its flight in the fireball. When the surrounding temperature is high enough, the 'radiative conduction', blowing and dissociation zones can be distinguished clearly in the profiles of the self-similar solution.

Some solution profiles are depicted in Fig. 3 where dimensionless temperature is plotted against the boundary layer similarity variable for three distinct cases. Heat transfer with low blowing (evaporation), transfer with blowing but without radiation and heat transfer by all mechanisms and involving blowing as well. In each curve one can distinguish three main regions. A region near the droplet surface where blowing is dominant and temperature changes are relatively mild; an intermediate region where the temperature is of 0(3000–4000 K) with steep changes and an inflection zone which reflect the dissociation process of the water molecules; and a region near the outer edge of the boundary layer in which the temperature gradients are low. This decrease is due to the dominance of heat transfer by radiation where heat flux is proportional to $T^3\,\partial T/\partial r$. The parametric ratio between heat transfer by conduction and radiation, N, which is expressed here using equation (8),

$$N = \frac{\Sigma k}{4\sigma T_\infty^3} = \frac{4}{3}\frac{\bar{q}_e}{\bar{q}_0}\frac{\bar{T}'_e}{\bar{T}_0} \tag{15}$$

plays a major role in determining the extent of the outer region and the associated temperature gradients there. Furthermore, this parameter actually characterizes the entire boundary layer. When N becomes larger the boundary layer is considered optically thick and transfer by conduction plays an increasing role.

Droplet evaporation rate

The evaporation rate of the droplet through the boundary layer is of the form

$$-\frac{\pi}{6}\frac{\mathrm{d}(D^3)}{\mathrm{d}t} = \frac{\pi}{2}\int_0^{\theta_{\max}} \rho_0 V_r(\theta) D^2 \sin\theta\,\mathrm{d}\theta \tag{16}$$

where

$$V_r = \frac{T_\infty k_0 r_k \bar{T}'(0) V_e}{2\mu_e}\left(\frac{\mu_e}{V_e x \rho_e}\right)^{0.5}. \tag{17}$$

The separation point was chosen to be at $\theta_{\max} = \pi/2$. We have assumed fore and aft symmetry for heat transfer with regard to that location similar to what is evident in Schlichting [17] for heat transfer to a cylinder perpendicular to the stream. Hence the droplet extinction rate can be presented as

$$-\frac{\mathrm{d}D}{\mathrm{d}t} = \frac{\sqrt{2}\rho_0 T_\infty k_0 V_e r_k \bar{T}'(0)}{\rho_L \lambda \mu_e}\left(\frac{\mu_e}{D\rho_e V_e}\right)^{0.5}. \tag{18}$$

The evaporation of the droplet involves processes with different typical time scales. The shortest scales are associated with adjustment within the boundary layer while the longest one is relevant to the rate of change of the drop diameter. A summary of the various scales involved is given in Table 1.

The time scale ratios were evaluated at 8 MPa and 8000 K for a 10^{-3}-m droplet moving at 100 m s^{-1}. These values suggest that droplet evaporation can be followed using a quasi-steady approach as was also suggested by [1].

The deceleration of the drop is given by

$$\frac{\mathrm{d}V_e}{\mathrm{d}t} = -\frac{3\rho_e V_e^2 C_d}{4D\rho_L} \tag{19}$$

where the steady-state drag coefficient is correlated by

$$C_D\begin{cases}\dfrac{27}{(Re_\infty + 2.5\,Re_r)^{0.84}} & 1 < Re_\infty < 100, \text{ref. [1]} \\ 0.29(1+9\,Re_\infty^{-0.5})^2 & Re_\infty > 100, \text{ref. [3]}.\end{cases} \tag{20}$$

In (20) Re_r is the Reynolds number associated with the blowing velocity. The droplet terminal velocity was estimated using [3] data

$$Re_\infty = \left\{\left(20.52 + \frac{2.135\,[D^3 g\rho_\infty(\rho_L - \rho_\infty)]^{1/2}}{\mu_\infty}\right)^{1/2} - 4.53\right\}^2. \tag{21}$$

The decay history of a single droplet in an isothermal field was calculated for various initial conditions. The results are compared to those of Golovin and Pesochin [1] and Harpole [3]. Since in our case, the transport properties of the steam undergo extreme changes in the dissociation range (3000–4000 K) the comparison is made at 8000 K, a typical initial temperature of the fireball at 8 MPa and beyond the dissociation zone. Figure 4 shows a plot of the Nusselt number vs $Re_\infty^{0.5} \cdot Pr_\infty^{0.33}$ for the three works. In this figure

Table 1. A comparison of time scales

Parameter	Typical time scale	Time scale within boundary layer	Time scale ratio
Velocity response	$\frac{D\rho_L}{\rho_\infty V_\infty C_D}$	$\frac{\delta_h^2 \rho_f}{\mu_f}$	$\frac{0.01\rho_L}{\rho_\infty C_p}$
Form response	$-D\Big/\frac{dD}{dt}$	$\frac{\delta_h}{V_\infty}$	100

radiation was not included in the calculation to enable a comparison. In the range relevant to this work ($10^2 < Re < 10^4$) all three correlations show a similar behavior. They deviate, however, at small Re due to the different approach to the influence of flowing on conduction.

Figures 5 and 6 show the dependence of the rate of change of a droplet diameter moving in an isothermal field on the ambient temperature and the operating pressure. dD/dt changes linearly with $P^{1/2}$ with the level of the curve increasing with increasing temperature. At a constant pressure the rate of evaporation increases monotonically with temperature. This augmentation is gradually decayed due to a formation of a blowing sublayer in which heat transfer is predominantly via conduction. Our calculations indicate that at high pressures the relative importance of transfer by radiation diminishes. Opacity to radiation becomes an important parameter which cannot be disregarded, at least for water vapor. This is similar to the role which a strong blowing plays in cases of evaporation by conduction and convection only [1, 3] where it limits the evaporation rate severely. The dependence of the contribution of radiation to evaporation rate on the instantaneous droplet diameter which appears in [1, 3] is not predicted by this solution. This difference stems from their assumption that the entire vapor is optically thin which yields a mixed dependence due to convective

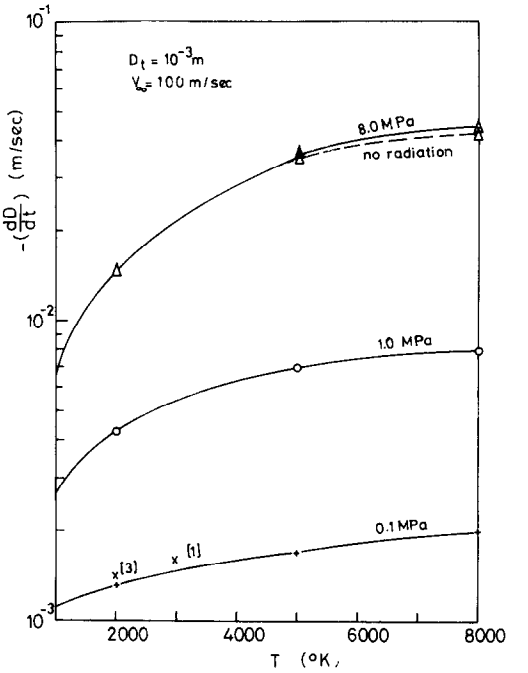

FIG. 5. The dependence of evaporation rate on temperature at various pressures.

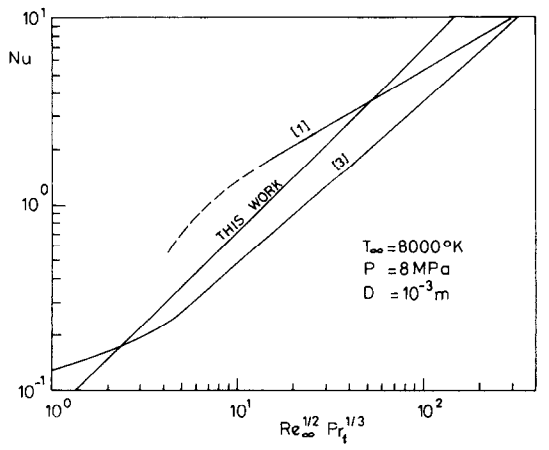

FIG. 4. A comparison between the model solution and literature correlations without radiation.

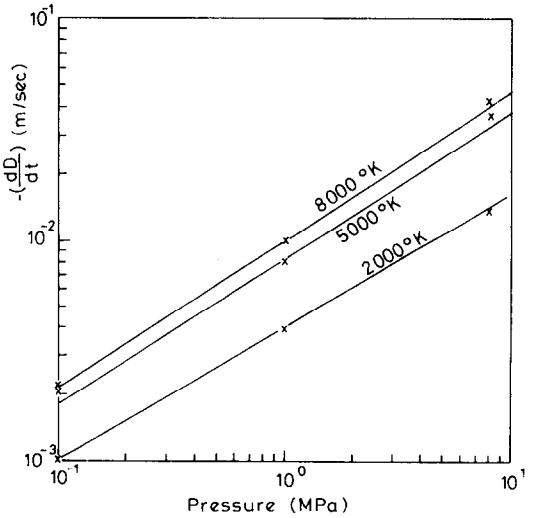

FIG. 6. The dependence of evaporation rate on pressure at various temperatures.

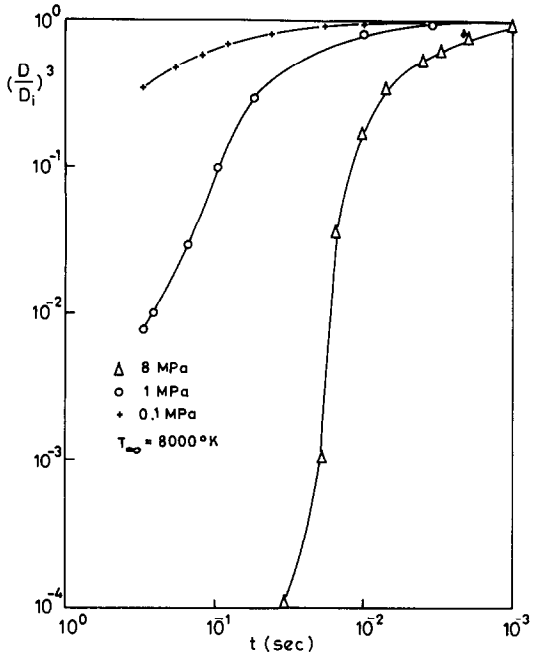

FIG. 7. The decrease of droplet volume with time.

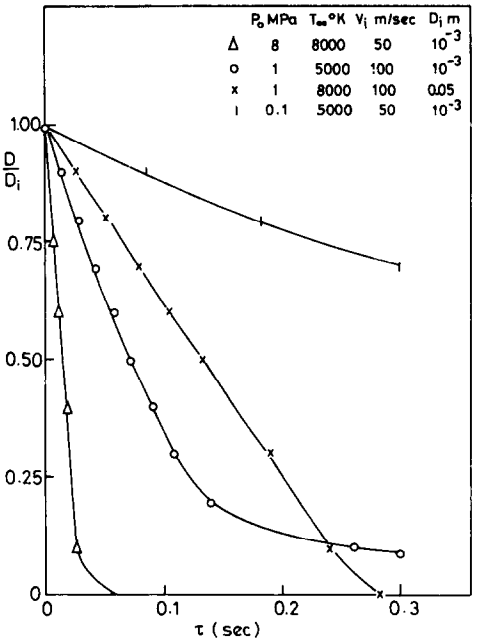

FIG. 8. The dependence of droplet diameter on time.

contribution $[0(D^{-0.5})]$ and a radiative transfer $[0(D^0)]$. When the boundary layer is optically thick the overall contribution is uniform and of $0(D^{-0.5})$.

The bulk contribution of a droplet to the adsorption of enthalpy in an isothermal field is realized during the initial small fraction of its existence time. This phenomenon is depicted in Fig. 7 for various pressures. It is interesting to note that, as can be seen in Fig. 8 the decrease of the droplet diameter is initially almost linear with time. A similar behavior was reported by Harpole [3] for droplets larger than 10^{-3} m. This constant rate of diameter change is a result of a decrease in evaporation rate due to the decreasing droplet velocity which is compensated by an increase in evaporation rate due to the diminishing size.

Fireball cooling rate

After studying the parameters governing the single droplet evaporation in an isothermal field it should prove interesting to estimate the fireball cooling process. This process involves changes in the ambient temperature surrounding each droplet and therefore is treated here using the quasi-steady approximation as in the previous section. Table 2 shows that such an approximation is well justified.

In order to simplify the cooling rate calculations we state some assumptions as follows:

(a) The fireball has homogeneous temperature and pressure during the cooling process.
(b) The fireball diameter is constant during cooling.
(c) All droplets enter the fireball with the same velocity.
(d) Gas motion in the fireball during cooling is neglected when compared with droplets typical velocity.
(e) The vapor swept from the droplets is mixed instantaneously with the fireball gas [18].
(f) The system fireball–droplets is adiabatic and in LTE [18].
(g) The assumptions relating to shape, integrity, trajectory and heat transfer mechanism associated with a single droplet hold also for their ensemble.

Table 2. Further comparison of time scales

Parameter	Typical time scale	Time scale within boundary layer	Time scale ratio
Temperature response	$\frac{\rho_e r_b^3}{dw/dt}$	$\frac{\delta_T^2}{\alpha_f}$	10^6

Assumption (a) implies that temperature homogenization of the fireball stems from dominance of radiation effects within the gas [12]. The fireball achieves an almost constant volume after 1 ms as can be approximated by the Taylor–Sedov point explosion theory and therefore remain practically unchanged during the entire cooling cycle. Assumption (c) is made for the convenience of the numerical evaluation. Assumptions (e) and (f) are consistent with assumption (a) and similar ones were previously invoked elsewhere [16].

The ensemble of droplets within the fireball has size and age distributions. Following [2] we have chosen an initial size distribution similar in shape to that measured in rockets, liquid propellant spray and an arbitrary residence time distribution.

$$\frac{\partial^2 S}{\partial D\,\partial t} = a_1 D^2 t \exp(-a_2 D^2 - a_3 t). \tag{22}$$

The parameter a_1 is associated with the total amount of water injected into the fireball during the entire cooling process. a_2 dictates the expectation of the droplets population diameter, i.e. $a_2 = 4/\pi\hat{D}^2$. a_3 indicates the time of maximum injection rate through $a_3 = 2\cdot\hat{t}^{-1}$. The total water mass entering the fireball during the cooling cycle is characterized by

$$A = \frac{3w_t\lambda}{4\pi r_b^3 \rho_\infty H_\infty}. \tag{23}$$

Fireball cooling was evaluated using the equation

$$\frac{dw}{dt} = -2\pi\rho_L \int_0^t \int_0^\infty R^2 \frac{dD}{dt_0}(D_0, T_\infty, R_i, t-t_0) \times \frac{\partial^2 S}{\partial R_i\,\partial t_0} dR_i\, dt_0 \tag{24}$$

where,

$$\frac{dH_\infty}{dt} = -\frac{3}{4}\frac{(H_\infty+\lambda)}{\pi r_b^3 \rho_\infty}\frac{dw}{dt}, \quad H_\infty = H_\infty(T_\infty). \tag{25}$$

In the numerical scheme the droplets population was discretized into 10 groups of various initial sizes each subdivided into 30 segments of different ages. Each group was followed from the moment of its introduction into the fireball at the initial velocity 100 m s^{-1} to the final time of calculation, i.e. 0.3 s. The calculation with respect to the droplet involved evaluation of their rate of evaporation using the boundary-layer equation described in the previous sections, and the decrease in droplets size and velocity. The following of each group is terminated in one of three situations: the group passes through and emerges out of the fireball, the diameter of the droplets became smaller than an arbitrary fraction (say 1/100) of its initial diameter; the temperature of the fireball decreased to 1 K above saturation temperature.

The pellet releases a certain amount of point explosion energy, 3×10^8 J. This energy dictates the initial diameter and temperature of the fireball,

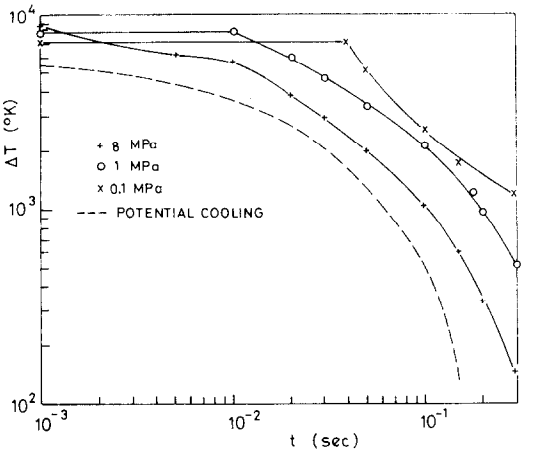

FIG. 9. Fireball cooling at various pressures, $A = 1$.

depending on the operating pressure. The transfer of water from liquid to vapor phase within the fireball and the associated consumption of latent heat of evaporation together with the increase of the gas mass serve as the mechanisms for the reduction of the fireball ambient temperature. Since the reactor volume as well as the working pressure are held constant, the fireball radius is proportional to $P^{-1/3}$. In this region, however, the volume remains unaltered due to the addition of water vapor.

The interesting parameters governing the cooling process are the operating pressure and the total mass of water injected into the fireball. A high pressure improves the cooling rate for two reasons: augmentation of the transport properties (e.g. thermal conductivity), within the boundary layer and an increase of the droplets residence time within the fireball due to a higher density. Figure 9 depicts the change of fireball temperature with time for different operating pressures. The curve associated with potential cooling is obtained assuming an instantaneous droplets evaporation and is obviously an upper bound for the cooling rate at a given total water mass. In drawing these curves we have used particular values for the parameters in equation (22) ($A = 1, a_2 = 2.5\times10^6$ m^{-2}, $a_3 = 10$ s^{-1}). These serve as an arbitrary demonstration only and their change will alter the figure quantitatively but less qualitatively. A shift in the size distribution may either compress all curves toward the potential curve or disperse them from it. It is evident that the rate of temperature change approaches the potential cooling rate as pressure increases. At high pressure most droplets do not pass through the fireball but rather keep on evaporating within it at their respective terminal velocity.

The total amount of water participating in the cooling cycle is defined in equation (23). Figure 10 shows the decrease of fireball temperature with time at 8 MPa for various values of the nondimensional water injection rate, A. The rate of temperature drop increases monotonically with A. However, the influence of A on

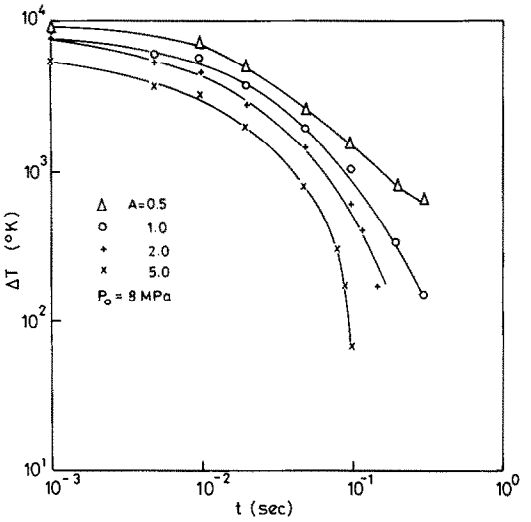

FIG. 10. Fireball cooling at 8 MPa for various total water loads.

the time required to achieve a final saturation temperature becomes minor at high pressures. Since droplets of most sizes participate in the cooling process and A is dominated by the mass of the larger ones. At low pressures its main contribution to cooling emerges from the fine spray and thus the dependence on A becomes more profound.

CONCLUSIONS

The velocity and temperature profiles within the boundary layer reflect the existence of the various sublayers associated with blowing, dissociation and radiation of water vapor. When radiation is absent we found good correspondence between known heat transfer correlations for relatively low temperatures and our calculations which takes dissociation into account. The ratio for radiation to convection contributions is overestimated when complete penetration is assumed. Lower ratios are obtained when vapor opacity at high pressures is considered. The quasi-steady assumption regarding the simultaneous processes associated with fireball cooling appear to be selfconsistent. It is evident that increasing the pressure augments the rate of the cooling process by both keeping the droplets within the fireball and increasing the instantaneous evaporation rate.

REFERENCES

1. A. M. Golovin and V. R. Pesochin, Evaporation of a drop of solution in a high temperature medium, *High Temp.* **14,** 720–727 (1976).
2. R. P. Hagerty, A. L. Jaumotte, O. Lutz and S. S. Pemmer, *High Temperature Phenomena*, pp. 158–159, 5th Agard Colloquium 4. Pergamon Press, London (1962).
3. G. M. Harpole, Radiative absorption by evaporating droplets, *Int. J. Heat Mass Transfer* **21,** 537–542 (1978).
4. H. Kislev, Pat. Pend. 62638 (Israel) (1981).
5. H. Kislev, Droplets evaporation by combined mechanisms in ICF reactor. M.Sc. thesis, Technion—Israel Institute of Technology, Haifa, Israel (1982).
6. H. Kislev and B. T. Micklich, 6th Topical Meeting on Fusion Engineering, San Francisco (1985).
7. S. Glasstone, The Effect of Nuclear Weapons, U.S. Atomic Energy Commission Review (1964).
8. T. F. Irvine and J. P. Hartnett, *Advances in Heat Transfer*, Vol. 5, pp. 254–321. Academic Press, New York (1968).
9. C. T. Dewey and J. F. Gross, Exact similar solutions of the laminar boundary layer equations, in *Advances in Heat Transfer*, Vol. **4,** pp. 317–446. Academic Press, New York (1967).
10. E. A. Gershbein, On outmoded numerical and asymptotic solutions of boundry-layer equations for high rate of injection. *Fluid Dynam.* **6,** 405–407 (1971).
11. L. A. Dombrovski, Radiative convective heat transfer in an optically thin boundary layer near the leading edge of a flat plate, *High Temp.* **15,** 885–891 (1977).
12. L. A. Dombrovski, Radiation convection heat transfer by an optically thick boundary layer on a plate, *High Temp.* **19,** 100–106 (1981).
13. F. H. Azad and M. P. Modest, Combined radiation and convection in absorbing emitting and anisotropically scattering as particulate tube flow, *Int. J. Heat Mass Transfer* **24,** 1681–1698 (1981).
14. G. B. Ludwig, Handbook of infrared thermal radiation of combustion gases, NASA-SP-3080, pp. 280–286 (1973).
15. E. R. C. Eckert and E. Pfender, Plasma heat transfer, in *Advances in Heat Transfer*. Academic Press, New York (1966).
16. A. Acrivos, The asymptotic form of the laminal boundary layer mass transfer rate for large interfacial velocity, *J. Fluid Mech.* **12** 337–370 (1962).
17. H. Schlichting, *Boundary Layer Theory*, p. 298. McGraw-Hill, London (1968).
18. L. A. Glenn, Transport processes in an inertial confinement fusion reactor. *Nucl. Engng Des.* **64,** 375–387 (1981).

EVAPORATION DE GOUTTELETTES PAR DES MECANISMES COMBINES DANS UN REACTEUR ICF

Résumé—Le transfert de chaleur entre un plasma de vapeur et une gouttelette d'eau sphérique et mobile est calculé en utilisant une solution de similitude pour une couche limite optiquement épaisse. On considère simultanément le rayonnement, la dissociation de la vapeur, la convection, la conduction et le soufflage. L'évaporation est calculée pour différentes pressions et températures et elle se compare bien avec des résultats à température basse et à la pression atmosphérique. Les résultats sont introduits dans un modèle qui décrit le mécanisme de refroidissement d'une boule de vapeur stagnante dans un réacteur ICF.

TRÖPFCHENVERDAMPFUNG BEI GLEICHZEITIGEM AUFTRETEN UNTERSCHIEDLICHER MECHANISMEN IN EINEM ICF-REAKTOR

Zusammenfassung—Der Wärmetransport von einem dichten Dampfplasma an ein bewegtes kugeliges Wassertröpfchen wurde für eine optisch dicke Grenzschicht berechnet. Das gleichzeitige Auftreten von Strahlung, Dampfdissoziation, Konvektion, Wärmeleitung und Einblasung wurde berücksichtigt. Für verschiedene Drücke und Temperaturen wurde die Tröpfchenverdampfungsrate berechnet, sie stimmt gut mit bekannten Verdampfungsraten bei niedrigen Temperaturen und Atmosphären-Druck überein. Die Ergebnisse wurden in ein Modell eingebaut, das den Kühlprozeß eines stagnierenden Dampffeuerballs, der für einen ICF-Reaktor vorausberechnet wurde, beschreibt.

ИСПАРЕНИЕ КАПЕЛЬ В РЕАКТОРЕ ICF, ВЫЗВАННОЕ ОДНОВРЕМЕННО ПРОТЕКАЮЩИМИ МЕХАНИЗМАМИ ПЕРЕНОСА ТЕПЛА

Аннотация—На основе автомодельного решения для оптически толстого пограничного слоя рассчитан теплоперенос от плазмы плотного пара к движущимся сферическим каплям воды. Рассматривались одновременно протекающие радиация, диссоциация пара, конвекция, теплопроводность и утечка. Скорость испарения капли, рассчитанная для различных значений давлений и температуры, хорошо согласуется с известными значениями при низких температуре и атмосферном давлении. Результаты использовались в модели, описывающей процесс охлаждения неподвижного парового болида, рассчитанного для реактора ICF.